

Enhanced Dynamic Energy Absorption in Carbon/Aramid Composite Tubes with Axially Graded Impedance

Saijod Tze Way Lau ^a, Chee Kuang Kok ^{b,*}, Md. Injamum Ul Haque ^b, Abdul Rahman Adenan ^c,
Sajid Abdullah Alam ^b, Sivakumar Dhar Malingam ^c, Purwo Kadarno ^d, Kia Wai Liew ^b

^a Compsits Enterprise, Taman Saujana Indah, 75450 Melaka, Malaysia

^b Centre for Advanced Mechanical and Green Technology, Faculty of Engineering and Technology, Multimedia University, Bukit Beruang, 75450 Melaka, Malaysia

^c Fakulti Kejuruteraan Mekanikal, Universiti Teknikal Malaysia Melaka, 76100 Durian Tunggal Melaka, Malaysia

^d Faculty of Industrial Technology, Universitas Pertamina, Kebayoran Lama, Jakarta 12220, Indonesia

Corresponding author: *ckkok@mmu.edu.my

Abstract— This study investigated the effects of carbon-aramid arrangement and strain rate on crush tube energy absorption. Round composite tubes, each consisting of three layers of fabric, were made using four different carbon-aramid hybridization schemes. Hand lay-up and compression bladder molding were used in the fabrication process. In two hybridization schemes, carbon-aramid fabrics were arranged to evaluate the effect of axially graded impedance relative to the tube impact end. Static crush and low-velocity impact (LVI) tests were conducted, and the force-displacement responses, energy absorption characteristics, and failure modes were compared. Test results revealed that energy absorption was 20% to 60% higher in the low-velocity impact test than in static crush, regardless of the hybridization schemes. In both tests, material arrangement played a surprisingly important role that was comparable to the tube carbon content in energy absorption. Maximum specific energy absorption of 26.21 kJ/kg was obtained in the hybridization scheme with the low impedance at the initiator end, with increasing impedance towards the impact end. This amount of specific energy absorption is almost equivalent to the other hybridization scheme that has twice the carbon fiber content. This scheme facilitated initial damage modes that favored progressive folding in the rest of the tube. This study presents the idea of enhancing the crashworthiness of crash boxes using axially graded impedance material arrangement. It is recommended that the idea be subjected to more testing for verification and potential commercialization.

Keywords—Hybrid composite tubes; static and dynamic crush; carbon-aramid system; graded material; crashworthiness.

Manuscript received 22 Nov. 2022; revised 17 Apr. 2023; accepted 8 Jul. 2023. Date of publication 31 Oct. 2023.
IJASEIT is licensed under a Creative Commons Attribution-Share Alike 4.0 International License.



I. INTRODUCTION

Composite crush tubes have been used in sports cars, trains, and helicopters to absorb impact energy by facilitating controlled structure destruction. However, their use has not been prevalent in normal passenger cars. This is because metallic crush structures are cheaper and easier to manufacture. With the increasing demand for sustainability requirements in automobiles, hybrid or battery electric vehicles are replacing conventional engine drive trains. This development comes with more stringent passive safety requirements, e.g., batteries placed in the boot of a vehicle should not deform in a rear impact. Composites, exhibiting higher specific properties than steel and aluminum can place metallic structures as an economical alternative [1].

Two general observations point to the possibility of graded material design in the composite for superior energy absorption. First, solid materials demonstrate the capacity to attenuate shock when arranged in decreasing impedance from the impact end [2]. Second, there is evidence of increased impact energy absorption in a tube where the impact end has a smaller effective diameter or thickness. Conversely, energy absorption is enhanced when a graded foam or honeycomb structure is impacted at its higher impedance end. Some natural materials, such as bamboo, display this impedance gradience by having a high density of cellulose fibers at the outer surface and a gradual lower density of the same towards the inner lignin region [3]. The advantage of graded material arrangement has yet to be harnessed in the use of hybridization of higher impedance carbon fiber with a typical density of 1.8 g/cm³ and stiffness of 183 GPa, and lower

impedance aramid with a typical density of 1.44 g/cm³ and stiffness of 76 GPa. It has been shown that carbon fabric has a significantly higher energy absorption capacity than aramid fabric. Tubes made of pure carbon fabric absorbed 20% more energy than a hybrid aramid-carbon tube when the difference in carbon volume fraction is a mere 4.3% [4]. Nonetheless, aramid fabric is essential for flexibility, elasticity, and the post-crush integrity of the tubes [5].

Investigations involving the hybridization of carbon and aramid fabrics in the composite tubes often involve consistent cross-sectional material lay-ups along their axes [6], or radially graded arrangement. Hybridization of carbon and aramid fabrics that occurs along the tube axis, as in a tube with multiple segments, is far less often reported. Isaac & Ezekwem [7] postulated that the lack of such a study stemmed from the difficulty in combining incompatible composite materials. Such axially graded hybridization may enhance energy absorption effectively, as has been shown by Alam et al. [8].

In crush tubes, impact energy absorption is often accomplished by dissipation through structural failures. Energy is best absorbed through failure mechanisms such as lamina crushing, transverse shearing, brittle fracturing, local buckling, and/or progressive folding [9]. Energy absorption can be in the form of frictional dissipation between laminate, fragmented debris wedge, bending and/or breaking of laminate bundles, splaying and frond bending, and inter-laminar crack-induced central delamination [6]. Important factors affecting energy absorptions are fiber and matrix properties, element geometry, the ratio of wall thickness to overall tube geometry, element arrangement/architecture, loading conditions such as crush speed, the use of initiator and trigger [10, 11], and fabrication method, which may have received the least attention [7]. An ideal crush tube should display stable, progressive crushing with its initial peak load being very close to its mean load, whose magnitude is maximized. Reduction of initial peak load is often accomplished by using triggers, whereas initiators induce the dominant failure modes, which greatly control the total energy absorption. Achieving this ideal requires careful design of both materials and structures. Important insights for overall superior performance include using round tubes, aligning carbon fiber to the crush axis and aramid fiber in hoop direction, placing carbon layers at inner layers and aramid at outer layers for hoop stress, etc. [7]. Woven fabrics do not supply as easily as unidirectional, providing better support to tube inner and outer walls than solid strengthening [5].

However, composite behavior can be difficult to predict when dealing with the specifics. For example, Ma et al. [6] found that round tubes of three layers (i.e., aramid/carbon/aramid) performed better in terms of energy absorption under quasi-static axial crush than those of five layers (i.e., aramid/carbon/aramid/carbon/aramid) by almost 4.5 times. The inward folding of a round carbon-epoxy tube with a chamfered end was found to increase the specific energy absorption by 82% and lowered the initial peak loads by 60% compared to the traditional outward splaying [12]. Yu et al. [13] showed how a variable structure could be utilized to flatten the force-displacement curve of inward-folding tubes if desired. In addition, heat treatment could lead to the shrinkage of the aramid fiber, which in turn induces bending

mode, often resulting in up to 67% increase in energy absorption in a carbon-aramid-epoxy material system [6]. However, temperature aging at 160°C could degrade the energy absorption of CFRP tubes by as much as 94% [14]. The use of epoxy-based resin doubled the impact energy absorption of carbon fiber-reinforced (CFR) tubes compared to vinyl ester-based resin [15]. Recent structural enhancements of crush tubes include origami-shaped tubes [16, 17] or origami prefolded cores [18], bio-inspired designs [19, 20], multi-layered walls, and nesting of tubes or fillings, made of either the same or other, sometimes advanced materials such as printed materials [21, 22, 23, 24, 25, 26, 27, 28, 29, 30]. These enhancements are often ahead of the commercial deployment, such as evidenced by Chen et al.'s [10, 31] recent report on their research and development efforts in characterizing hybridized CFRP/GFRP crash boxes with the end goal of providing practical guidelines for Chang Chun Railways Vehicle Co.

Considering that there have been very few investigations on the hybridization of carbon and aramid fabrics that occurs along the tube axis, this study aimed to evaluate the effects of strain rate on the specific energy absorption and crush load response in round crush tubes with axially graded impedance. The composite tubes were subjected to static crush and low-velocity impact tests.

II. MATERIAL AND METHOD

A. Materials and Samples

Plain weave carbon fiber fabric (ACG Composite, sized 3K, 1000D, A grade, 200 gsm) and aramid fiber fabric (ACG Composite, sized 3K, 1000D, 200gsm) were purchased from Jiaying Newtex Composites Co., Ltd., China. The vendor reported the carbon fiber fabric's tensile modulus and tensile strength as 230 GPa and 3530 MPa, respectively. Typical aramid fiber fabric of almost identical technical specification has a tensile modulus and tensile strength of around 100 GPa and 2.4 GPa, respectively [32]. The epoxy used is clear Picarbon epoxy with a curing time of 12 hours from Picarbon Malaysia.

Hand lay-up and compression bladder molding techniques were used to fabricate the composite tubes. Details of fabrication can be obtained in Alam et al. [8]. Fabrics were cut to sizes and then impregnated with epoxy. They were wrapped around a silicone bladder in a mold to form layers. During molding, the bladder was pressurized to 7 bars such that the outer dimensions of the specimens conformed with the mold shape. After more than 24 hours of curing, the specimens were removed from the mold. The round hollow composite tube specimens are 51 mm outer diameter, 0.85 ± 0.02 mm thick, and 100 ± 6 mm long. The fiber orientations for all samples made in this study were 0°/90°. Four different material lay-ups were employed, as shown in Figure 1. Four specimens were made for each hybridization scheme (i.e., I, II, III, and IV). Two specimens were subjected to a static crush test and two to a low-velocity impact test.

Tubes of hybridization scheme I have a carbon-to-aramid fabric mass ratio of 2:1, whereas the rest of the tubes have a carbon-to-aramid fabric mass ratio of 1:2. This scheme serves as a reference for carbon-dominated hybrid tubes. Material arrangement in hybridization scheme II was benchmarked

against Ma et al. [6], despite their being filament wound tubes. This scheme serves as a reference for aramid-dominated hybrid tubes. Materials in hybridization scheme III were arranged in increasing impedance axially from the impact end, whereas those in hybridization scheme IV were arranged in decreasing impedance. Hybridization schemes III and IV are identical in material arrangement but different in the end loading conditions. These two schemes are meant to investigate the effects of axially graded stiffness in static loading and impedance in dynamic loading, respectively. The tube fiber weight fraction ranges from 0.58 to 0.62. The carbon and aramid fabric volume fractions, respectively, are 32% and 19% for hybridization scheme I, and 16% and 37% for other hybridization schemes.

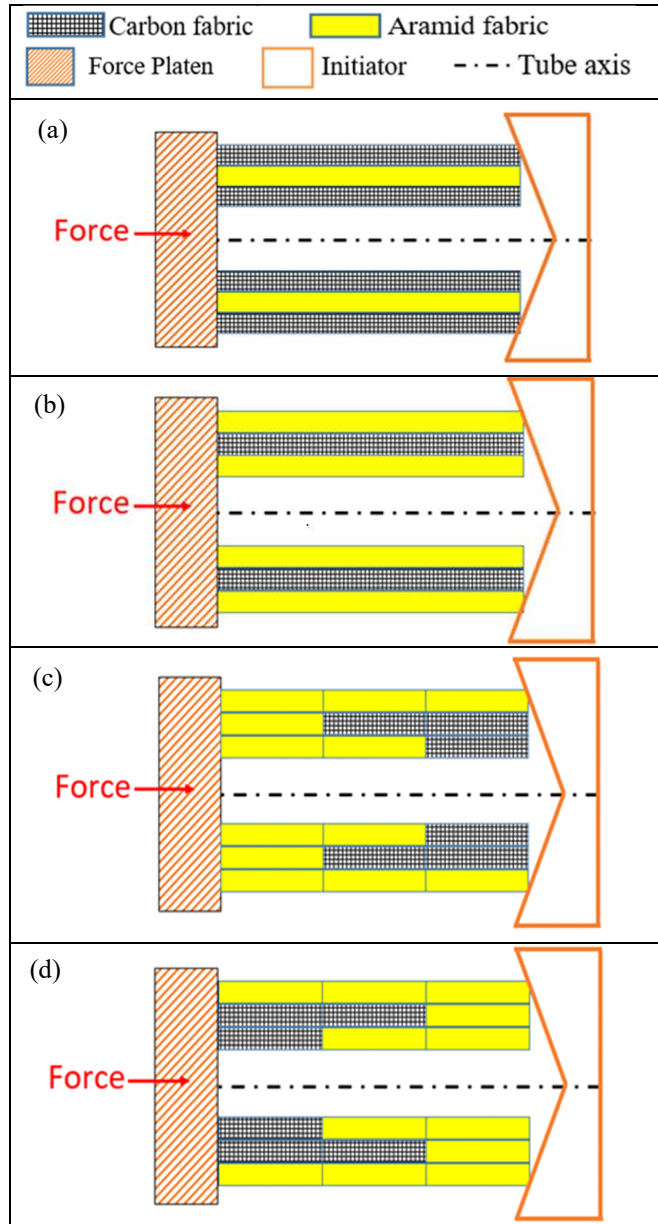


Fig. 1 Material lay-ups in four different hybridization schemes (I-IV). (a) I; (b) II; (c) III; (d) IV

In transitioning from two dissimilar fabrics, the fabrics were overlapped slightly for about 1.5 cm to mitigate the effects of fiber discontinuity and to facilitate the fabrication

of graded material. The fabricated composite tube was then allowed to cure for 24 hours at ambient temperature before removal from the mould. The moulded tubes are presented in Figure 2.



Fig. 2 Moulded tubes ready for crush tests of hybridization schemes of I to IV, from left to right

B. Static Crush and Dynamic Impact Tests

Instron 3367, with a capacity of 30 kN was used to conduct the static crush test at a speed of 5 mm/min per ASTM D695. A typical test setup is shown in Figure 3(a).

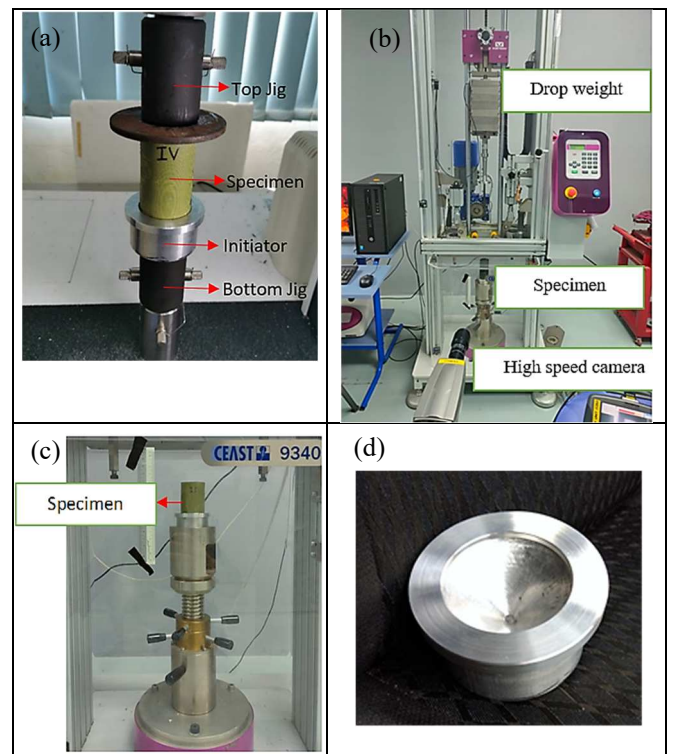


Fig. 3 (a) Static crush test experimental setup; (b) Low-velocity impact test setup; (c) Specimen holder of the LVI; (d) Initiator and its cavity

Low-velocity impact (LVI) test was conducted using Instron CEAST 9340 drop tower at a drop height of 0.999 m, a total drop weight of 38.1 kg (including the mass of the tup and tup holder, as well as the impact jig), making the impact equivalent to 373 J and the before impact speed 4.43 m/s. The experimental setup can be seen in Figures 3(b) and 3(c). The tube was centrally placed (Figure 3(c)) within the cavity of the initiator without any other constraints. The tubes were then crushed upon dropping the mass following a typical drop test procedure displayed in other works [5, 33]. A high-speed camera (Olympus i-speed 2 CDU) captured the deformation upon the drop impact. The initiator cavity is shaped like an inverted cone with a slope of 45° (Figure 3(d)) to facilitate the inward folding of the tubes.

The initial peak load for each crush test was recorded. The crush load efficiency (CLE) (i.e., a ratio of mean load to peak load that indicates crushing stability) and the specific energy absorption (SEA) were computed as described by Alam et al. [8]. In computing the energy, the densification stage of the force-displacement curve was excluded. Crushed tubes were inspected, and different failure modes and their locations were identified.

III. RESULT AND DISCUSSION

To simplify the presentation and further discussion, the tubes are designated in “scheme (sample number)”, i.e., “I(S1)” is sample 1 of hybridization scheme I.

A. Results

Figures 4(a) and 4(b) summarize the force-displacement responses in static and LVI axial crush tests, respectively.

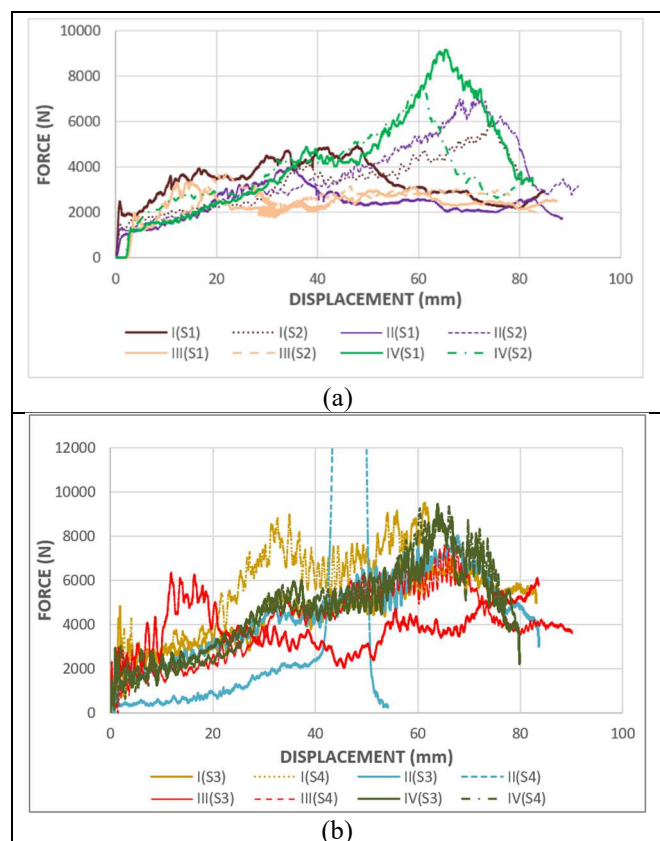


Fig. 4 Force-displacement responses of all tubes in (a) static; and (b) LVI axial crush tests, respectively

Table 1 summarizes the energy absorption, and the crush load efficiency of the hybrid crush tubes in the static crush and LVI tests for the different hybridization schemes. The tubes' static and LVI crush force-displacement responses were also superimposed in Figure 5, according to the different hybridization schemes. The post-crush morphology of the tubes in the static crush and LVI tests are presented in Figure 6 and Figure 7, respectively. Overall, the hybrid composite tubes absorb more energy under the LVI test. For the most part, the characteristics and modes of failures under the dynamic impact test do not differ much from those under the static crush test. Significant differences will be highlighted and described in Section 4.3.

TABLE I
ENERGY ABSORPTION AND CRUSH LOAD EFFICIENCY OF THE HYBRID CRUSH TUBES IN THE STATIC CRUSH AND LVI TESTS FOR THE DIFFERENT HYBRIDIZATION SCHEMES

Scheme	Test	Crush Length (mm)*	Average EA (J)	Average SEA (kJ/kg)	Average CLE
I	Static	80.2 (S1),	271.20	20.16	0.62
		80.8 (S2)			
II	Static	80.8 (S1),	263.19	18.41	0.57
		91.6 (S2)			
III	Static	87.4 (S1),	209.12	13.63	0.68
		83.7 (S2)			
IV	Static	82.6 (S1),	319.40	21.81	0.48
		76.3 (S2)			
I	LVI	83.1 (S3),	360.03	26.06	0.61
		62.2 (S4)			
II	LVI	83.6 (S3)	371.83	25.02	0.55
		83.6 (S3),			
III	LVI	90.1 (S4)	341.39	21.86	0.56
		83.6 (S3),			
IV	LVI	79.8 (S3),	370.94	26.21	0.50
		79.1 (S4)			

*Taken at the initiation of densification. Peaks due to catastrophic failure were ignored.

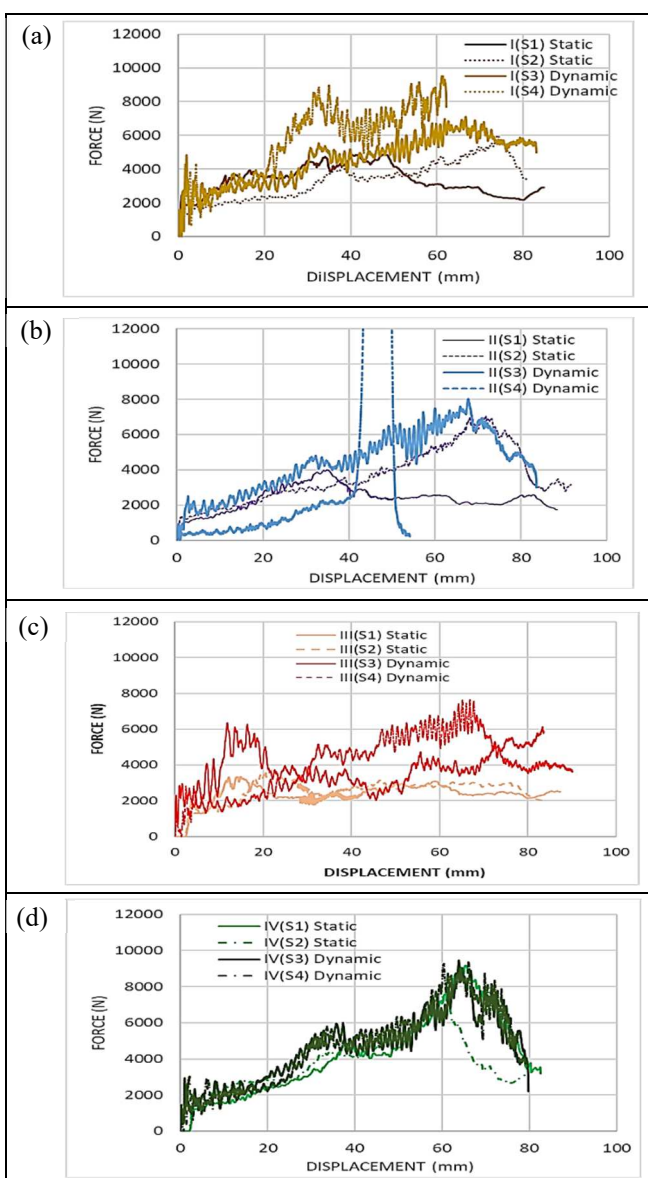


Fig. 5 Force-displacement responses of all tubes in (a) static; and (b) LVI axial crush tests, respectively

Sample Name	Top View	Bottom View	3D or Side View	Failure Mode
I(S1)				Longitudinal crack; fracture at seam, delamination.
I(S2)				Longitudinal crack, fragmentation, progressive folding; fracture at the seam.
II(S1)				Global buckling and local buckling; delamination; fracture at the seam.
II(S2)				Progressive folding; small fracture at the seam.
III(S1)				Top stretching and localized folding; fracture at the seam.
III(S2)				Top stretching and localized folding; fracture at the seam.
IV(S1)				Progressive folding at the bottom, and single fold at the top; fracture at the seam.
IV(S2)				Progressive folding at the bottom, and single fold at the top; fracture at the seam.

Fig. 6 Failure modes of all hybridization schemes in static crush test. Longitudinal cracks and seam fractures were highlighted in red circles.

B. Discussion

1) *Static Crush*: Figure 5 shows that the trends of the force-displacement responses between samples of the hybrid tubes in static crushing were mostly consistent in hybridization schemes III and IV. In schemes I and II, deviations in the responses between samples started at a crush length of about 40 mm to 50 mm and were attributed to the difference between the slant mode and the straight-in mode, as illustrated in Figure 8(a) and Figure 8(b), respectively. In a typical slant mode, such as exhibited by I (S1), the inward folding of the tube segment in the initiator could not proceed further, causing the tube to twist and slant slightly. The non-uniform inward folding of the bottom segment of the tube

most likely caused the slant. This slanting was believed to have led to the tube top/impact end stretching into an oblong shape and a gradual subsequent off-axis crushing of the tubes. Imagine that the tube consists of four equal quadrants, as illustrated in Figure 9.

Sample Name	Top View	Bottom View	3D or Side View	Failure Mode
I(S3)				Global buckling; some extent of progressive folding at the bottom; fragmentation.
I(S4)				Global buckling; limited bottom-up progressive folding; fragmentation; fracture at the seam.
II(S3)				Progressive folding; fracture at seam; delamination.
II(S4)				Global buckling induced sideways crush catastrophic failure; delamination.
III(S3)				Global buckling and localized folding; longitudinal crack; fracture at seam fragmentation.
III(S4)				Progressive and localized folding; lamina bending; fracture at the seam.
IV(S3)				Progressive folding, fragmentation.
IV(S4)				Progressive folding, fragmentation.

Fig. 7 Failure modes of all hybridization schemes in the LVI test. Longitudinal cracks and seam fractures were highlighted in red circles

During the non-homogeneous deformation, the local weakness at the bottom of the tube led to major inward folding predominantly in one quadrant or in two opposite quadrants, as demonstrated in the bottom row of Figure 9. This led to a

slight slant of the tube as well as stiffening of the tube bottom at the major fold(s). As the crushing force continued, the stiffer bottom fold(s) compelled the neighboring material at their immediate upper row to bulge inwards, and that together with the downward moving top jig stretched the tube top in the direction perpendicular to the major fold lines, forming the oblong opening. The slant eventually contributed to the local folding at the oblongated top, as illustrated in the top and middle rows of Figure 9. Since this failure mode was rather nondeterministic, the resulting crush forces between I(S1) and I(S2) differed. As I(S2) did not exhibit this failure mode but “straight-in” mode, it also absorbed more energy. In a straight-in mode, the tube bottom inward folding was uniform, and the tube crushed into the initiator almost vertically, often by progressive folding.

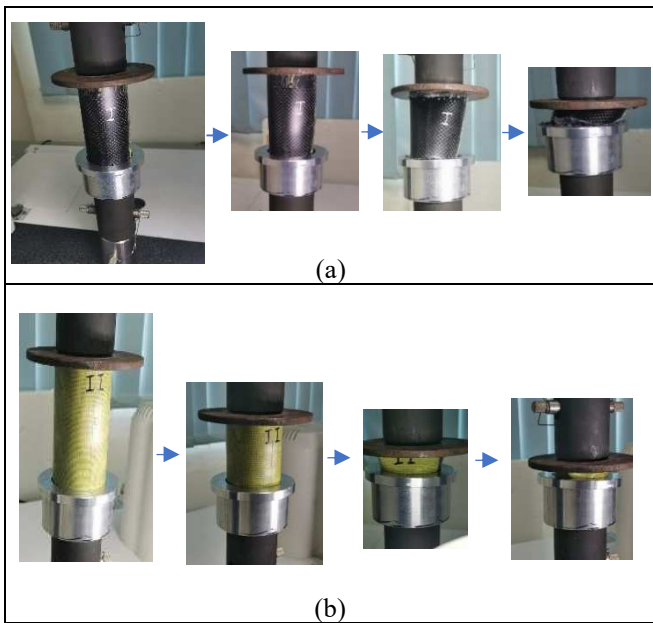


Fig. 8 (a) Tube slanting and oblongated tube top led to off-axis crushing of I(S1); (b) Straight-in with progressive folding of II(S2)

II(S1) exhibited the slant mode similar to I(S1), but II(S2) went straight into the initiator, displaying the progressive folding that favored higher energy absorption, despite the top stretching towards the end of the crush, as in Figure 6(b), and it absorbed more energy than II(S1). It is clear from this observation in the deviation of static crush responses between I(S1) and I(S2), and between II(S1) and II(S2) that there exists the possibility of different failure modes in composite tubes of the same material composition. The differences are undesirable and have stemmed primarily from the loose constraint in the inward crush procedure. During the test, the tube solely rested on the contacting surfaces between the tube end and the initiator cavity without any other constraints. An ideal specimen of perfect cylindricity, uniformity, and edge flatness would have crushed straight downwards and displayed uniform inward folding. Apparently, the specimens in this study do not meet such ideality in shape and form. On the other hand, the authors refrained from implementing artificial constraints, such as the use of temporary fixtures on the tube ends, to minimize potential distortion of the experimental data. Viewing from another perspective, these differences in crush responses allude to the opportunity to

induce better consistency in tube crush responses by altering the material lay-up. Such improved consistency in the static crush responses was indeed observed in tubes of hybridization schemes III and IV, which featured axially graded stiffness.

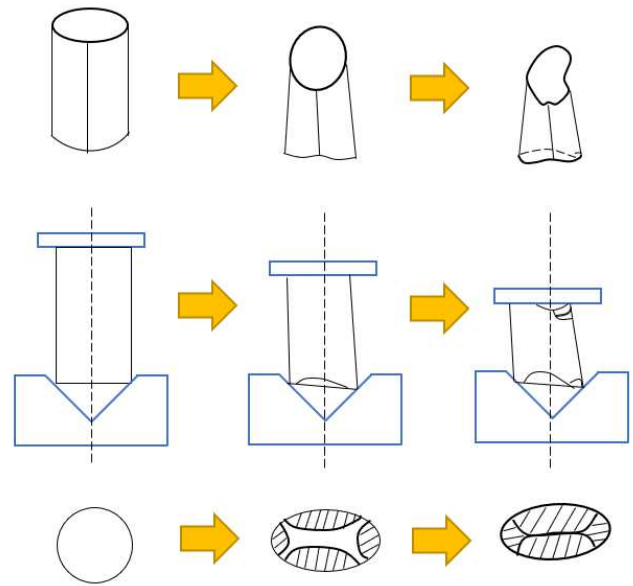


Fig. 9 Failure mechanism leading to certain tubes' oblongated top and bottom during static crush. The top row depicts the three-dimensional view of the tube, the mid row its side view, and the bottom row its bottom view

Hybridization scheme III consistently underperformed in energy absorption. The relatively high impedance carbon at the initiator end of hybridization scheme III made it difficult for the tubes to fold inwards and with uniformity. With the low impedance aramid segment stretching at the impact end, the deformation modes of III(S1) and III(S2) were similar to those of I(S1) and II(S1). On the other hand, the relatively low impedance at the initiator end of hybridization scheme IV led to the ease of inward folding and facilitated the desirable “straight-in” crushing as in II(S2). A single local folding at the top sometimes accompanied the progressive bottom-up folding of the tube. These desirable failure modes also displayed a gradual increase in crushing force as the crushing proceeded from the bottom segment (~33 mm) to the middle segment (~67 mm), before dropping off in the last segment (see Figure 5(d)). The gradual increase of load up to over 70 mm, or 7/10 of crush length in hybridization scheme IV tubes was an exceptional and often sought-after optimized response to maximize crashworthiness [9].

2) *Dynamic Impact:* Figure 5 clearly shows that for all samples regardless of hybridization schemes, the crush forces in the LVI test were higher than those in the static crush test by 20% to 60%. II(S4), which failed catastrophically and hence excluded from the comparison, was the exception. A greater energy absorption was evidenced under loading at a higher strain rate, as tabled in Table 1. This is surprising as many findings on axially crushed homogeneous composite tubes reported in the literature indicated otherwise [4, 34, 35]. Nevertheless, the literature [36] seemed to be inconclusive regarding the effect of strain rate on the axially homogeneous tubes. II(S4)'s global buckling induced catastrophic failure in the LVI test, as illustrated in Figure 4(b) and Figure 5(b),

featured a sudden peak load, flattening at the limit of 47.28 kN (not shown) and then dropped to near zero. II(S4)'s unstable deformation mode differed significantly from IIS3's progressive folding. Such inconsistent performance from one sample to the next was also observed in tubes of carbon-carbon system in Littell et al. [33] and is greatly undesirable, as it can lead to reliability issues. Again, the prime suspect for such inconsistency in this work is the loose constraint in the inward crush procedure. Subsequently, the reported values in Table 1 represent only the samples without catastrophic failure.

The higher strain rate or extra energy in the impact seemed to have caused the bottom segments of the tubes to deform and conform to the initiator profile more easily, such that the tubes remained straight, thereby crushing the tubes straight into the initiator. This remained true even for tubes of hybridization scheme III, whose top segments were pure aramid, which were too compliant to resist the impact. These tubes displayed undesirable post-failure oblongated tops, no less severe than their counterparts in a static test. Figure 10 depicts the dynamic crushing of selected tubes as captured by the high-speed camera.

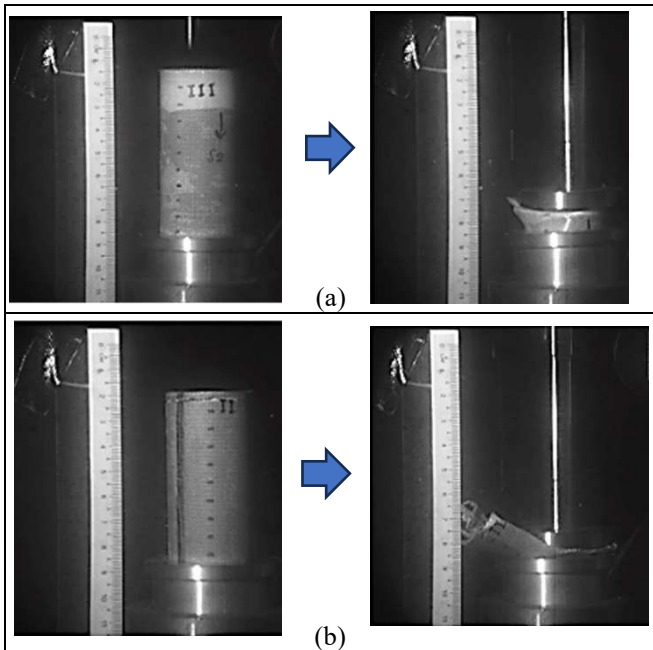


Fig. 10 Tube deformation in LVI test. (a) Straight-in mode of III(S4)—notice the oblongated top; (b) Slanting and catastrophic failures in II(S4)

Clearly, the catastrophic failure in II(S4) had to do with tube slanting that led to the toppling of the tubes. And slanting happened due to non-uniform bottom folding. It is worth noting that the failure mechanism illustrated in Figure 9 may not fully apply to II(S4), as there was insufficient time to develop the bottom-folding-induced inward bulge fully before the tubes toppled. Instead, the impact weight fell on the tube as it lay sideways.

3) *Post-failure Morphology and Energy Absorption:* There was a significant but gradual bounce-back or length recovery of certain tubes after force removal in the static crush and LVI tests, consistent with Littell et al. [33]. The failure modes and energy absorption appeared to correlate strongly

with the material arrangement in the tube segments concerning the impact end and the initiator/stationary end. In terms of energy absorption, it is a known fact that progressive folding tends to perform better than fractures and delamination, and global buckling is the least desirable. Coincidentally, longitudinal fracture could be observed in samples of hybridization scheme I where the outer layer of the impacted top segment was carbon, along with some degree of progressive folding. Samples of hybridization scheme II demonstrated unstable crush behavior II(S4) catastrophically failed during dynamic crush, and II(S1) exhibited global buckling in static crushing. This seemed to imply that hybridization scheme II is predisposed to underperform in an axial crush. Nevertheless, samples of hybridization scheme III were the worst performers. Except for III(S4), their great resistance to bottom folding and weak top segments that were oblongated during the impact rendered the tubes susceptible to top stretching, global buckling, and localized folding. Carbon fiber fragmentation was common in all tubes, even in tubes that were wrapped by an outer aramid layer. Powdery carbon fiber debris easily detached from these samples. Longitudinal cracks and seam fractures were observable mostly in samples of hybridization schemes I, II, and III.

Samples of hybridization scheme IV seemed to outperform other samples in energy absorption, as the low stiffness or impedance material at the initiator end facilitated initial inward folding that propagated upwards. The gradual transitioning of material to higher stiffness or impedance at the impact end also prevented the possibility of global buckling at the uncrushed segment of the tubes. Despite having only half the carbon content of hybridization scheme I, the performance of hybridization scheme IV was at par with or slightly better than hybridization scheme I, highlighting the importance of material arrangement in inducing failure modes favorable to energy absorption. The SEA values of 21.81 kJ/kg in the static test and 26.21 kJ/kg in the dynamic test compare favourably with the 29.66 kJ/kg in the static test achieved by Ma et al. [37] whose specimen is a 2-layer filament wound round carbon fibre reinforced plastic tube of an outer diameter of 41.6 mm and thickness of 1.2 mm, supported with an inner polylactic acid tube.

IV. CONCLUSION

The dynamic crushing of the hybrid tubes exhibited higher energy absorption in the range of 20%-60% than the static crushing in all hybridization schemes, except when catastrophic failures occurred. In both static crush and dynamic impact, the initiator inducing inward folding of the tube end exerted much influence on the subsequent tube failure beyond the initial stages and the overall failure mode of the tubes. Tubes that displayed progressive folding under static crush did so under dynamic impact because of the initial inward folding at the initiator. Poor material arrangement can lead to unstable performance, such as catastrophic failures in the form of global buckling, as witnessed in IIS4 in dynamic impact. To facilitate energy absorption with the initiator, the results showed that it is better to have the lower impedance material at the initiator end where inward folding first occurred, as in hybridization scheme IV. The impedance can then be increased in a graded manner towards the impact end for enhanced energy absorption. Doing this can result in

enhancing dynamic energy absorption that is almost equivalent to doubling the carbon content, as evidenced by the comparable energy absorption in the specimens of schemes I and IV in this study. Of all the hybridization schemes, scheme IV displayed the best specific energy absorption of 21.81 kJ/kg in the static test and 26.21 kJ/kg in the dynamic test. It is recommended that the idea of enhancing the crashworthiness of crash boxes using axially graded impedance material arrangement, such as presented in this work, be subjected to further testing for commercial development.

ACKNOWLEDGMENT

This work was supported by the Universitas Pertamina-Multimedia University Collaborative Research Award 2021 (MMUE/210001). The authors are grateful for the support.

REFERENCES

- [1] D. Lukaszewicz, "Automotive Composite Structures for Crashworthiness," in *Advanced Composite Materials for Automotive Applications: Structural Integrity and Crashworthiness*, New Jersey, Wiley, 2013, pp. 99-127.
- [2] D. Hui and P. Dutta, "A new concept of shock mitigation by impedance-graded materials," *Compos. B*, vol. 42, p. 2181-2184, Dec. 2011, doi: 10.1016/j.compositesb.2011.05.016.
- [3] F. Xu, X. Zhang and H. Zhang, "A review on functionally graded structures and materials for energy absorption," *Engr. Struct.*, vol. 171, p. 309-325, Sep. 2018, doi: 10.1016/j.engstruct.2018.05.094.
- [4] J. Xu, Y. Ma, Q. Zhang, T. Sugahara, Y. Yang and H. Hamada, "Crashworthiness of carbon fiber hybrid composite tubes molded by filament winding," *Compos. Struct.*, vol. 139, pp. 130-140, Apr. 2016, doi: 10.1016/j.compstruct.2015.11.053.
- [5] J. Chambe, C. Bouvet, O. Dorival and J. Ferrero, "Energy absorption capacity of composite thin-wall circular tubes under axial crushing with different trigger initiations," *J. Compos. Mater.*, vol. 54, no. 10, pp. 1281-1304, Sep. 2019, doi: 10.1177/0021998319877221.
- [6] Y. Ma, T. Sugahara, Yang, Y. and H. Hamada, "A study on the energy absorption properties of carbon/aramid fiber filament winding composite tube," *Compos. Struct.*, vol. 123, pp. 301-311, May 2015, doi: 10.1016/j.compstruct.2014.12.067.
- [7] C. Isaac and C. Ezekwem, "A review of the crashworthiness performance of energy absorbing composite structure within the context of materials, manufacturing and maintenance for sustainability," *Compos. Struct.*, vol. 257, no. 113081, Feb. 2021, doi: 10.1016/j.compstruct.2020.113081.
- [8] S. Alam, C.K. Kok, S.T.W. Lau, A.R. Adenan, M.I.U. Haque, S.D. Malingam, P. Kadarno and G.M. Chen, "Inward crushing of square and round carbon/aramid multiple-segment tubes under axial quasi-static loading," *Compos. Struct.*, Vols. 311, Article 116826, pp. 1-12, Feb. 2023, doi: 10.1016/j.compstruct.2023.116826.
- [9] G. Jacob, J. Fellers, S. Simunovic and J. Starbuck, "Energy Absorption in Polymer Composites for Automotive Crashworthiness," *J. Compos. Mater.*, vol. 36, no. 7, pp. 813-850, Apr. 2002, doi: 10.1177/002199830203600716.
- [10] D. Chen, Y. Liu, M. Meng, B. Li, X. Sun, B. Yang, S. Xiao and W. T., "Dynamic axial crushing behaviors of circular composite tubes with different reinforcing fibers and triggers," *Int. J. Mech. Sci.*, vol. 244, p. 108083, Apr. 2023, doi: 10.1016/j.ijmecsci.2022.108083.
- [11] M.N. Hussain, S.P. Regalla and Y.V.D. Rao, "Study on influence of notch triggers on absorption of energy for composite automobile crash box under impact loads," *Materials Today: Proceedings*, vol. 38, no. 5, pp. 3220-3231, Mar. 2021, doi: 10.1016/j.matpr.2020.09.715.
- [12] D. Siromani, G. Henderson, D. Mikita, K. Mirarchi, R. Park, J. Smolko, J. Awerbuch and T.-M. Tan, "An experimental study on the effect of failure trigger mechanisms on the energy absorption capability of CFRP tubes under axial compression," *Compos. A*, vol. 64, pp. 25-35, Sep. 2014, doi: 10.1016/j.compositesa.2014.04.019.
- [13] Z. Yu, X. Zhou, X. Zhou, Y. Zhang and Q. Zhu, "Crashworthy subfloor structure of civil aircraft via inclined inward-folding composite tubes," *Compos. B*, vol. 189, p. 107887, May 2020, doi: 10.1016/j.compositesb.2020.107887.
- [14] W. Zuo, Q. Luo, Q. Li and G. Sun, "Effect of thermal and hydrothermal aging on the crashworthiness of carbon fiber reinforced plastic composite tubes," *Compos. Struct.*, vol. 303, p. 116136, Jan. 2023, doi: 10.1016/j.compstruct.2022.116136.
- [15] J. Gupta, N. Reynolds, T. Chiciudean and K. Kendall, "A comparative study between epoxy and vinyl ester CF-SMC for high volume automotive composite crash structures," *Compos. Struct.*, vol. 244, p. 112299, Jul. 2020, doi: 10.1016/j.compstruct.2020.112299.
- [16] A. Ciampaglia, D. Fiumarella, C. Boursier Niutta, R. Ciardiello and G. Belingardi, "Impact response of an origami-shaped composite crash box: Experimental analysis and numerical optimization," *Compos. Struct.*, vol. 256, p. 113093, Jan. 2021, doi: 10.1016/j.compstruct.2020.113093.
- [17] Z. Song, S. Ming, K. Du, C. Zhou, Y. Wang, S. Xu and B. Wang, "Energy absorption of metal-composite hybrid tubes with a diamond origami pattern," *Thin-walled Struct.*, vol. 180, p. 109824, Nov. 2022, doi: 10.1016/j.tws.2022.109824.
- [18] K. Huang, H. Ye, Z. Yu and X. Zhou, "Energy absorption properties of composite sandwich tubes with pre-folded cores," *Compos. Struct.*, vol. 294, p. 115737, Aug. 2022, doi: 10.1016/j.compstruct.2022.115737.
- [19] Y. Duan, T. Zhang, J. Zhou, H. Xiao, X. Chen, M. Al Teneiji, Z.W. Guan and W.J. Cantwell, "Energy-absorbing characteristics of hollow-cylindrical hierarchical honeycomb composite tubes inspired a beetle forewing," *Compos. Struct.*, vol. 278, p. 114637, Dec. 2021, doi: 10.1016/j.compstruct.2021.114637.
- [20] J. Xing, J. Zhao, Q. Niu, T. Zhang, C. Zhang, Y. Zhang, W. Wang, S. Yan and X. Liu, "Crashworthiness design and optimization of bamboo-inspired tube with gradient multi-cells," *Thin-Walled Struct.*, vol. 191, p. 111034, Oct. 2023, doi: 10.1016/j.tws.2023.111034.
- [21] N. Abdullah, M. Sani, M. Salwani and N. Husain, "A review on crashworthiness studies of crash box structure," *Thin-walled Struct.*, vol. 153, p. 106795, Aug. 2020, doi: 10.1016/j.tws.2020.106795.
- [22] T.A. Sebaey, D.K. Rajak and H. Mehboub, "Internally stiffened foam-filled carbon fiber reinforced composite tubes under impact loading for energy absorption applications," *Compos. Struct.*, vol. 255, p. 112910, Jan. 2021, doi: 10.1016/j.compstruct.2020.112910.
- [23] D. Meriç and H. Gedikli, "Multi-objective optimization of energy absorbing behavior of foam-filled hybrid composite tubes," *Compos. Struct.*, vol. 279, p. 114771, Jan. 2022, doi: 10.1016/j.compstruct.2021.114771.
- [24] W. Hou, P. He, Y. Yang and L. Sang, "Crashworthiness optimization of crash box with 3D-printed lattice structures," *Int. J. Mech. Sci.*, vol. 247, p. 108198, Jun. 2023, doi: 10.1016/j.ijmecsci.2023.108198.
- [25] I. Ozen, H. Gedikli and M. Aslan, "Experimental and numerical investigation on energy absorbing characteristics of empty and cellular filled composite crash boxes," *Engr. Struct.*, vol. 289, p. 116315, Aug. 2023, doi: 10.1016/j.engstruct.2023.116315.
- [26] C. Yang, Z. Chen, S. Yao, P. Xu, S. Li and M.S. Alqahtani, "Quasi-static and low-velocity axial crushing of polyurethane foam-filled aluminium/CFRP composite tubes: An experimental study," *Compos. Struct.*, vol. 299, p. 116083, Nov. 2022, doi: 10.1016/j.compstruct.2022.116083.
- [27] Y. Deng, Y. Ren, X. Fu and H. Jiang, "Bionic-bamboo design for enhancing the crashworthiness of composite tube with groove trigger subjected to oblique load," *Int. J. Mech. Sci.*, vol. 206, p. 106635, Sep. 2021, doi: 10.1016/j.ijmecsci.2021.106635.
- [28] S.F. Hwang, C.-Y. Wu and H.-K. Liu, "Crashworthiness of Aluminum-Composite Hybrid Tubes," *App. Compos. Mater.*, vol. 28, p. 409-426, Feb. 2021, doi: 10.1007/s10443-020-09851-1.
- [29] H. Yang, H. Lei and G. Lu, "Crashworthiness of circular fiber reinforced plastic tubes filled with composite skeletons/aluminum foam under drop-weight impact loading," *Thin-Walled Struct.*, vol. 160, p. 107380, Mar. 2021, doi: 10.1016/j.tws.2020.107380.
- [30] H. Alshahrani, B. Almeshari, M.A. Abd El-baky and T.A. Sebaey, "Crashworthiness assessment of foam-filled internally strengthened carbon fibre-reinforced composite tubes under axial compression," *Int. J. Crashworthiness*, Apr. 2023, doi: 10.1080/13588265.2023.2198832.
- [31] D. Chen, X. Sun, B. Li, Y. Liu, T. Zhu and S. Xiao, "On Crashworthiness and Energy-Absorbing Mechanisms of Thick CFRP Structures for Railway Vehicles," *Polymers*, vol. 14, p. 4795, Nov. 2022, doi: 10.3390/polym14224795.
- [32] M. Moure, N. Feito, J. Aranda-Ruiz, J. Loya and M. Rodriguez-Millan, "On the characterization and modelling of high-performance para-aramid fabrics," *Compos. Struct.*, vol. 212, p. 326-337, Mar. 2019, doi: 10.1016/j.compstruct.2019.01.049.

- [33] J. Littell, J. Putnam and R. Hardy, "The Evaluation of Composite Energy Absorbers for use in UAM eVTOL Vehicle Impact Attenuation," in *VFS 75th Annual Forum and Technology Display*, Philadelphia, Pennsylvania, 2019. [Online]. Available: <https://core.ac.uk/download/pdf/323103972.pdf>.
- [34] Y. Wang, J. Feng, J. Wu and D. Hu, "Effects of fiber orientation and wall thickness on energy absorption characteristics of carbon-reinforced composite tubes under different loading conditions," *Compos. Struct.*, vol. 153, pp. 356-368, Oct. 2016, doi: 10.1016/j.compstruct.2016.06.033.
- [35] G. Rzyńska and R. Gieleta, "Effect of Test Velocity on the Specific Energy Absorption under Progressive Crushing of Composite Tubes," *Adv. Sci. Tech. Res. J.*, vol. 14, no. 2, p. 94–102, Jun. 2020, doi: 10.12913/22998624/118551.
- [36] J.-E. Chambe, C. Bouvet, O. Dorival, S. Rivallant and J.-F. Ferrero, "Effects of dynamics and trigger on energy absorption of composite tubes during axial crushing," *Int. J. Crashworthiness*, vol. 26, no. 5, pp. 549-567, Apr. 2020, doi: 10.1080/13588265.2020.1766175.
- [37] Q. Ma, I. Sahat, M. Mat Rejab, S. Hassan, B. Zhang and M. Merzuki, "The energy-absorbing characteristics of filament wound hybrid carbon fiber-reinforced plastic/polylactic acid tubes with different infill pattern structures," *J. Reinf. Plast. Compos.*, vol. 38, no. 23-24, p. 1067–1088, Aug. 2019, doi: 10.1177/0731684419868018.